# Development of Heat Pipe Code for Extended Safety Analysis of Heat Pipe Reactor

Seojun Park, Kyung Mo Kim*
*Department of Energy Engineering, Korea Institute of Energy Technology (KENTECH), Kentech-gil 21, Naju-si, Jeollanam-do 58330, Republic of Korea*
*seojun@kentech.ac.kr, kmokim@kentech.ac.kr*

***Keywords: Heat pipe reactor, Alkali-metal heat pipe, Safety Analysis, Computational code, Passive system**

## 1. Introduction

Heat Pipe Microreactor (HPR), which use heat pipes to cool the core, can exclude the use of coolants (fluids), can be operated with or without gravity, and can be microminiaturized unlike conventional reactors, it is evaluated as optimized technologies for the extreme conditions. The latest developments in small reactor technology have been led by the United States, with DOE and the Department of Defense (DOD) conducting aggressive research and development, including the Microreactor Program (MRP) and Project Pele, in collaboration with national laboratories and private companies. The United States has already developed experimental nuclear satellite SNAP-10A in 1965 and conducted orbit operation it. With the reemergence of the micronuclear reactor technology concept in the 2010s, it is currently (2020s) entering the stage of demonstration and commercialization. Therefore, Korea is also promoting the development of space reactors to supply power to the lunar habitat. However, in order to develop a domestic heat pipe reactor, it is necessary to prove the safety of the reactor by performing safety analysis through the development of computational analysis technology for the heat transfer performance of the heat pipe corresponding to the reactor coolant system (RCS) of light water reactors. While the existing heat pipe codes have predictive performance for priming conditions, the actual heat pipe design and operating conditions may differ depending on the reactor and environment. Therefore, this study is developing a computational analysis code that can calculate the heat transfer performance of heat pipes for various heat pipe designs and operating conditions.

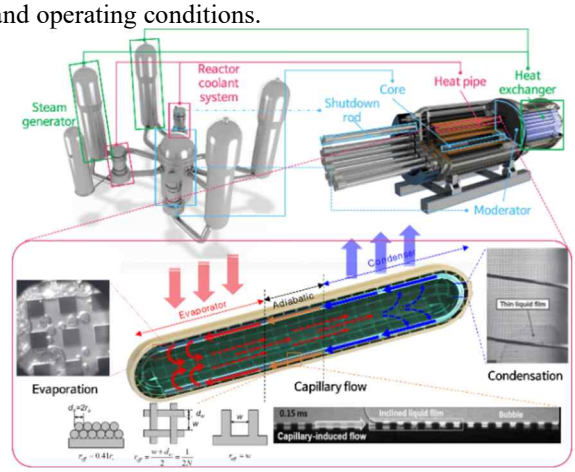


Fig. 1. Heat Pipe Reactor Structure

## 2. Heat Pipe In-house Code

The heat pipe computational analysis code developed in this study is based on the one-dimensional thermal resistance network. As shown in figure 2 and figure 3, the code was developed as a framework of an algorithm that performs heat transfer performance analysis based on thermal resistance circuits according to boundary conditions, design geometry, and working fluid properties. Then it calculates the maximum heat transfer capacity (operating limit) and predicts the actual heat transfer amount by determining whether the heat transfer design requirements for the heat conduit design geometry are met.

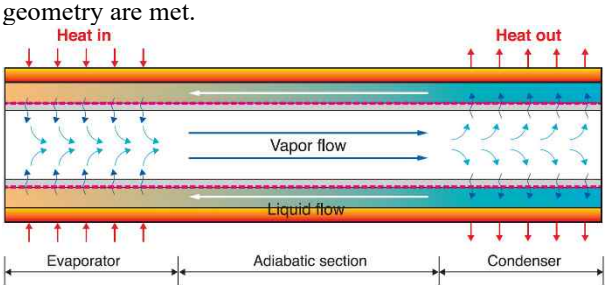


Fig. 2. Heat Pipe Modeling Structure [2]

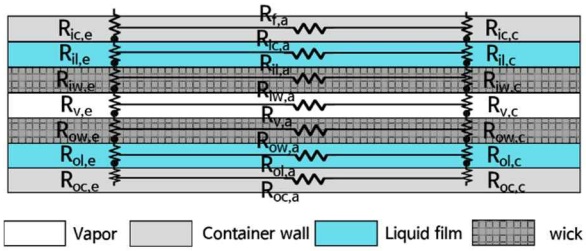


Fig. 3. Heat Pipe Computer Modeling Structure

*The detailed model for organizing the code was written in 2.1~2.4.*

### *2.1. Wick Parameter*

The wick parameters were composed of effective capillary radius, porosity, permeability, and effective thermal conductivity [1, 3].

Effective capillary radius $r_c$ decides maximum capillary pressure $\Delta P_{c,m\,ax}$ as follows:

$$\Delta P_{c,m\,ax} = \frac{2\sigma}{r_c} \quad (1)$$

where $\sigma$ = surface tension especially sodium.

Porosity $\epsilon$ which is ratio of voids to total volume works as parameter that determine permeability. Representatively, the permeability of screen wick $K$ follows modified Blake-Kozeny correlation:

$$K = \frac{d^2\epsilon^3}{C(1-\epsilon)^3} \quad (2)$$

where $d$ = a wire radius, $C$ = constant according to the wick types.

Effective thermal conductivity $k_{eff}$ is determined by a mixture of thermal conductivity of wick solid metal and liquid sodium. The effective thermal conductivity of screen wick is defined as follows:

$$k_{eff} = \frac{k_l[(k_l+k_s)-(1-\epsilon)(k_l-k_s)]}{[(k_l+k_s)+(1-\epsilon)(k_l-k_s)]} \quad (3)$$

where $\epsilon$ = porosity, $k_l$ = liquid sodium thermal conductivity and $k_s$ = wick solid metal thermal conductivity.

### *2.2. Pressure Drop*

The pressure drop was divided into liquid flow pressure drop and vapor flow pressure drop [1, 2].

Liquid flow on wicks could be considered as laminar flow. The pressure drop along the length of the wick is:

$$\frac{dP_l}{dx} = -\frac{2\tau_l}{r_{h,l}} - \rho_l g \sin\theta \quad (4)$$

where $\tau_l$ = frictional stress at the liquid/solid interface, $r_{h,l}$ = hydraulic radius, $\theta$ = heat conduction tube gradient, $\rho_l$ = liquid sodium density and $g$ = gravitational acceleration.

The sodium liquid vapor produced in the evaporation section travels along to the condensation section. Vapor flow pressure drop is:

$$\frac{dP_v}{dx} = -\frac{(f_v Re_v)\mu_v \dot{m}_v}{2A_v r_v^2 \rho_v} - \beta \frac{2\dot{m}_v}{A_v^2 \rho_v}\frac{d\dot{m}_v}{dx} \quad (5)$$

where $A_v$ = vapor flow path area, $r_v$ = vapor flow path radius, $f_v$ = vapor friction coefficient, $Re_v$ = vapor flow Reynolds number, $\mu_v$ = vapor viscosity, $\dot{m}_v$ = vapor mass flow rate and $\rho_v$ = vapor density. $\beta$ is a coefficient to account for the effect of vapor velocity variations within the vapor flow cross section, the following is defined:

$$\beta = \frac{\rho_v^2 A_v}{\dot{m}_v^2}\int_{A_v} V_v^2\, dA \quad (6)$$

### *2.3. Temperature Distribution*

The temperature distribution model was operated with thermal resistance model, transient model and Quasi-Steady-State model [1, 2].

The code calculates the thermal resistance between evaporator, condenser, pipe, wick and vapor. Using a transient model, it calculates the temperature distribution when condition states are changed, for example, reactor's output change or cooling condition change situation. For connect to reactor core thermal fluid code, Quasi-Steady-State Model were used.

### *2.4. Operational limits*

The operational limits considered were capillary limit, sonic limit, viscous limit, boiling limit [1, 3].

The working fluid driving force in a heat conduit is the capillary force at the wick. So, the entire pressure loss cannot be over the maximum capillary force. The capillary limit that is heat transfer rate when the entire pressure loss is equal to maximum capillary force is shown as follows:

$$\Delta P_{c,max} = \Delta P_l(Q_{cap}) + \Delta P_v(Q_{cap}) \quad (7)$$

where $\Delta P_{c,max}$ = maximum capillary pressure, $\Delta P_l$ = liquid sodium pressure loss and $\Delta P_v$ = capillary limit.

Vapor flow in a heat conduction tube is accelerated at the evaporating section and flows through the insulating section. On these sections, vapor flow velocity cannot over the speed of sound. The heat transfer when the velocity of the vapor flow is equal to the speed of sound is called the sonic limit and it is shown as follows:

$$Q_{sonic} = A_v \rho_v h_{fg}\left[\frac{\gamma R T_v}{2(\gamma+1)}\right]^{0.5} \quad (8)$$

where $A_v$ = vapor flow cross-sectional area, $\rho_v$ = vapor density, $h_{fg}$ = heat of vaporization, $\gamma$ = sodium vapor specific heat ratio, $T_v$ is sodium vapor absolute temperature.

Total pressure loss of sodium vapor cannot exceed the sodium vapor pressure at condenser section. If the heat transfer rate is too high or the operation temperature is too low, the pressure difference becomes lower and viscous effect becomes strengthened. And it would more likely reach viscous limit that sodium vapor cannot move. LUPHIS code uses the following calculation formula:

$$Q_{visc} = \frac{d_v^2 A_v h_{fg}}{64\mu_v L_{eff}}\rho_v P_v \quad (9)$$

where $Q_{visc}$ = viscous limit, $d_v$ = vapor flow diameter, $A_v$ = vapor flow cross-sectional area, $h_{fg}$ = heat of vaporization, $\mu_v$ = vapor viscosity, $L_{eff}$ = effective heat transfer length of the heat pipe, $\rho_v$ = vapor density and $P_v$ = vapor pressure.

On the evaporation section, boiling limit occurs when vapor bubbles interrupt the heat transfer on wick interface. Boiling limit calculates as follows:

$$Q_{boil} \frac{2\pi L_e k_e T_v}{h_{fg}\rho_v \ln(r_o/r_i)}(2\sigma)\left(\frac{1}{r_n}-\frac{1}{r_c}\right) \quad (11)$$

where $L_e$ = evaporator length, $k_e$ = effective thermal conductivity of wick, $r_o$ = outer radius of wick, $r_i$ = inner radius of wick, $r_n$ = nucleate boiling radius and $r_c$ = capillary radius of wick.

## 3. Results and Discussion

Using the developed in-house code, the heat transfer performance, especially for the operation limit ($Q_{max}$), of the heat pipe in various length of the adiabatic section was calculated to demonstrate its analysis performance. The detailed information of the heat pipe geometry investigated by the code is summarized in Table 1.

Table I: The detailed information of the hate pipe geometry

| | |
|---|---|
| Length(evaporator) | 0.25 m |
| Length(adiabatic) | 0.5 ~ 5.0 m |
| Length(condenser) | 0.25 m |
| Tube diameter | 0.0191 m |
| Tube thickness | 0.0012 m |

| | |
|---|---|
| Tube thermal conductivity | 16.2W/m-K |
| Initial operating temperature | 1023K |
| Heating power | 500W |
| Coolant bult temperature | 703K |
| Effective heat transfer coefficient | 100W/m^2-K |
| Tube angle | 0 radian |
| Gravity | 9.8 m/s$^2$ |

The following is the simulation result graph of the operating limit for temperature $T$ when the adiabatic length is 1.0m, 2.5m, and 5.0m.

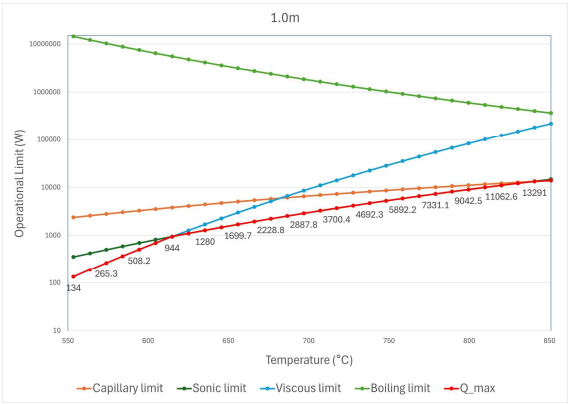


(a) adiabatic length = 1.0 m

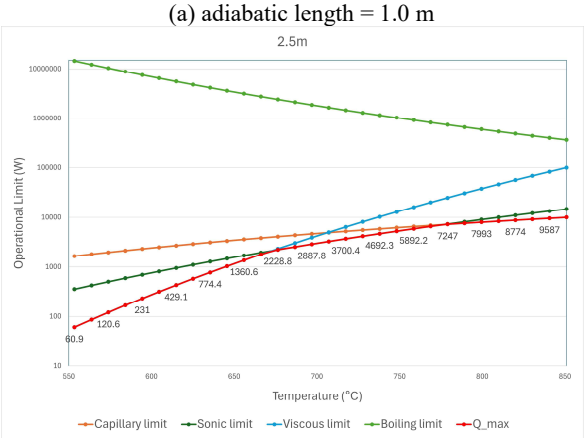


(b) adiabatic length = 2.5 m

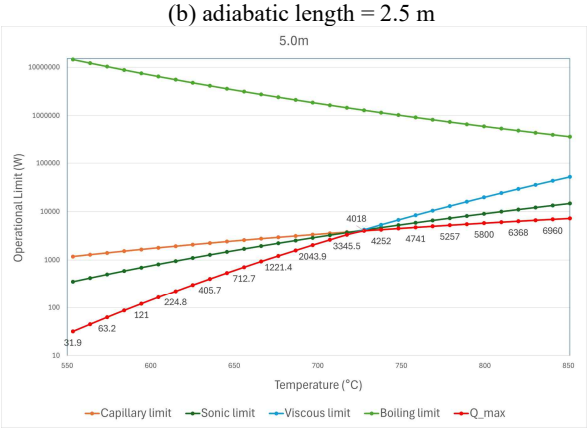


(c) adiabatic length = 5.0 m

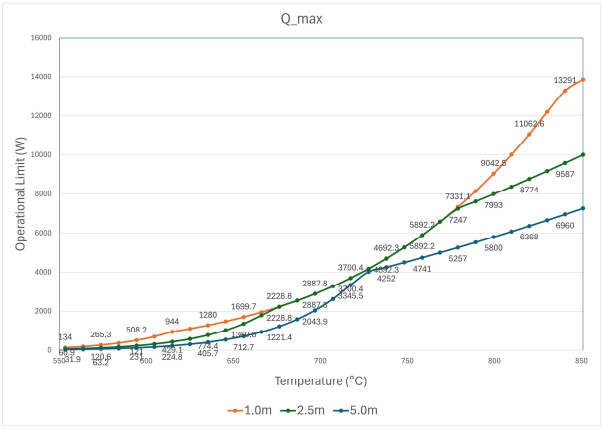


(d) Total

Fig. 4. Estimated operational limit of the heat pipe according to different adiabatic length (1.0, 2.5, and 5.0 m)

Fig. 4 is the graph of changing operational limit of the heat pipe according to different adiabatic length. On the relatively low vapor temperature (operational temperature) section, it was observed that operational limit was determined by viscous limit, and above a certain vapor temperature, it was determined by capillary limit. As shown in Fig. 4(d), it was observed that the difference at viscous limit by different adiabatic length, and it was shown that, as adiabatic length was decreased, viscous limit was decreased, and operational limit was increased. This was a result of the change in the effective length in Eq. (9), it proves that the change in the viscous limit according to the heat pipe adiabatic length is properly interpreted.

## 4. Future Work – Modeling of Two-Phase Flow

Although the existing codes including the currently developed code in this study have the reasonable capability on the heat pipe performance, they have limitations predicting the change of the heat pipe performance according to the amount of working fluid charged because the effect of the liquid film thickness (void fraction) is not considered and the interfacial area between the vapor core and liquid film is assumed as an inner diameter of the wick. According to the previous studies, the fill ratio of the working fluid remarkably affects the effective thermal conductivity and operation limit. Therefore, the code should be updated to account for void fraction; the effect of the fill ratio by considering the variation of heat conduction and interfacial areas with the thickness of the liquid film.

According to Sockeye by Hansel et al. [6], void fraction $a_v$ which is the effect of the working fluid fill rate was considered on the model. Void fraction affects the contact angle of the liquid-vapor interface, and it affects again to the capillary pressure $\Delta p_{cap}$ and the interfacial area density $a_{int}$. Void fraction $a_v$ is represented on 3 types by the interface position of the liquid-vaper. The interface is flat at the inner wick surface in Fig. 5. (a) was expressed as $a_v^{wick,i,0}$. If it is at

the inner wick surface in Fig. 5. (b), it expressed as $a_v^{wick,i,+}$, and if it is at the outer wick surface in Fig. 5. (c), it expressed as $a_v^{wick,o,+}$. $a_v^{wick,i,+}$ and $a_v^{wick,o,+}$ was assumed that it has hemispherical vapor pore volumes receding into wick.

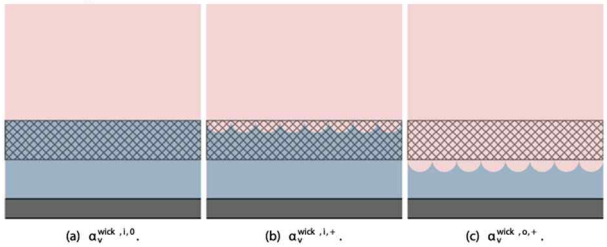


Fig. 5. Three types of void fraction bound illustration [6]

On the simulation code, the void fraction was calculated with functions about the pore site density and the geometric relation of the void volume of pore by the four range of three types of void fraction bound: when $a_v$ is under $a_v^{wick,i,0}$, when $a_v$ is more than $a_v^{wick,i,0}$ and under $a_v^{wick,i,+}$, when $a_v$ is more than $a_v^{wick,i,+}$ and under $a_v^{wick,o,+}$, and when $a_v$ is more than $a_v^{wick,o,+}$.

The capillary pressure difference between phases is a function of the capillary radius:

$$\Delta P_{cap}(a_v) = \begin{cases} 0 & \xi = 1 \\ \dfrac{2\sigma}{R_{cap}(\xi)} & \xi \neq 1 \end{cases}. \qquad (12)$$

The interfacial area density $a_{int}$ represents the surface area of the liquid-vapor interface per unit flow volume. The void fraction functions as parameter of the interfacial area density $a_{int}$. It is mainly affected by void fraction, or the pore site density function and it also differs by the range of $a_v$.

## 5. Summary

For the development of a Heat Pipe Microreactor (HPR) optimized for application in extreme environment reactors, we are developing a heat pipe performance analysis code that is essential to demonstrate the safety of the reactor on virtual accident experiment. Accordingly, in this study, a one-dimensional thermal resistance network code was developed by referring to the previous heat pipe code research results, and the performance of the code was evaluated through analysis of the adiabatic length change conditions and analysis of the results. In the future, we plan to upgrade the code to implement the impact of hydraulic phenomena, including fill ratio, on heat pipe performance, and this would be expected to be applied to advance reactor design and analyzing heat pipe reactor safety by providing accurate analysis results for various virtual accident scenarios and heat pipe designs.

## ACKNOWLEDGEMENT

This work was supported by the KENTECH Research Grant (202300006A) and R&D planning program supported by Jeonnam TechnoPark.

## REFERENCES

[1] N. Tak, S.N. Lee and C.S. Kim, Development of Computer Code for Performance Analysis of Heat Pipe of a Space Nuclear Reactor, KAERI/TR-8116/2020, 2020.
[2] C. Byon, Heat Pipe and Phase Change Heat Transfer Technologies for Electronics Cooling, Electronics Cooling. InTech, Jun. 15, 2016.
[3] N. Tak and S.N. Lee, Transient Lumped Parameter Analysis of Heat Pipe for a Space Nuclear Reactor, Transactions of the Korean Nuclear Society Virtual Spring Meeting, July 9-10, 2020.
[4] D.H. Lee, I.C. Bang, Dry-out limit enhancement strategy in sodium heat pipes: Overfilling effect and modified capillary limit model, International Journal of Heat and Mass Transfer, Volume 228, 2024.
[5] D.H. Lee, I.C. Bang, Experimental investigation of thermal behavior of overfilled sodium heat pipe, International Journal of Heat and Mass Transfer, Volume 215, 2023.
[6] J. E. Hansel, R. A. Berry, D. Andrs, M. S. Kunick, and R. C. Martineau, "Sockeye: A one-dimensional, two-phase, compressible flow heat pipe application," Nuclear Technology, vol. 207, no. 7, pp. 1096–1117, Jul. 2021.